Direct Numerical Simulation of Jet in Crossflow actuators

B. Selent[1] and U. Rist[1]

Institut für Aerodynamik und Gasdynamik, Universität Stuttgart, Pfaffenwaldring 21, D-70550 Stuttgart, Germany, email: lastname@iag.uni-stuttgart.de

Summary. Jet vortex generators have been proven to provide a mechanism to positively control boundary layer flows. The present paper illustrates a method to perform direct numerical simulations (DNS) of a jet actuator flow inside a laminar boundary layer. A structured finite difference method is used for the simulations. The numerical scheme was adapted to account for the large scale differences both in geometric and fluid dynamic aspects. Analytical mesh transformations have been implemented to resolve the jet orifice. Suitable boundary conditions are established to model the jet flow. Arising numerical instabilities have been suppressed by implementing a compact filter scheme. Test simulations are done for jet actuator configurations in laminar baseflow with jet to freestream velocity ratios of up to $R = 3.0$. The computational effort on a NEC SX 8/9 is also investigated.

1 Introduction

Jet actuators or jet vortex generators have been proven to provide a mechanism to positively control boundary layer (BL) flows. Experimental work by Johnston et al. [7] has shown the general ability to suppress separation in flows with adverse pressure gradients. The effect stems from the fact that longitudinal vortices are established inside the boundary layer and a mixing of the BL's faster layers with low-speed layers closer to the wall takes place. The mixing in turn leads to increased skin friction thus enabling the flow to overcome larger pressure gradients in downstream direction. This is a very similar effect observed from passive vortex generators [4]. The advantage of jet vortex generator systems over existing solid generators lies in their flexibility to be applied only when necessary and thus to avoid any parasitic drag. An exhaustive parameter study was undertaken by Godard et al. [6] covering many aspects of jet actuators such as velocity ratio R, skew angle β and pitch angle α, hole geometry and direction of rotation.

Albeit the outcomes of these experiments yield a very good general idea of the mechanisms of active flow control devices there are still a number of open questions involved as no detailed picture of the formation of the vortex and its interaction with the boundary layer could be gained from experiment yet. Therefore, any design suggestions for actuators rely heavily on empirical data and are difficult to transpose

to different configurations. Within the present research numerical simulations of jet actuators are to be performed by means of the DNS technique. The DNS approach is used for its lack of any model assumptions. Therefore, it is well suited to provide a reference solution for coarser or "more approxiamtive" numerical schemes. Furthermore, DNS allows for a computation of the unsteady flow formation especially in the beginning of the vortex generation and detailed analysis of the fluid dynamics involved.

2 Numerical Method

2.1 General setup

The numerical simulations are based on the complete Navier-Stokes equations for fully compressible, transient and three-dimensional flow. The computational domain consists of a flat plate and is depicted in figure 1. Simulations start with initial con-

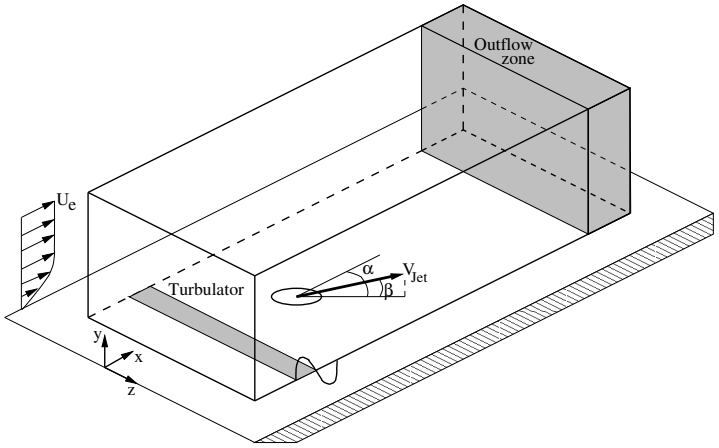

Fig. 1. Computational domain

ditions for a laminar baseflow and allow for the introduction of harmonic sinusoidal perturbations through a turbulator strip as well as discrete jet-disturbances through a round hole or slit. The jets can be skewed to the freestream by an arbitrary angle α and inclined by an angle β relative to the flat plate. The outflow contains a sponge zone where all perturbations are ramped to zero values. The code *NS3D* [1] solves the NS equations written in conservative variables [10]

$$\mathbf{Q} = [\rho, \rho u, \rho v, \rho w, E]^T.$$

In terms of the solution vector $\mathbf{Q}$ and the according flux vectors $\mathbf{F}$, $\mathbf{G}$, $\mathbf{H}$ the basic equation to be solved becomes

$$\frac{\partial \mathbf{Q}}{\partial t} + \frac{\partial \mathbf{F}}{\partial x} + \frac{\partial \mathbf{G}}{\partial y} + \frac{\partial \mathbf{H}}{\partial z} = 0.$$

Time integration of the base equation is carried out by a standard four-step Runge-Kutta method of order Δt^4. In order to stabilize the simulation the stencil used to compute the spatial derivatives can be shifted forward and backward at each sub step of the Runge-Kutta integration in order to add increased numerical viscosity.

The spatial derivatives in downstream and wall-normal direction (x,y) are approximated by compact finite differences with spectral-like resolution of order h^6 [9]. The resulting tridiagonal linear systems of equations are solved by the Thomas algorithm. In spanwise direction z a Fourier spectral method is implemented to approximate spatial derivatives. (Inverse)FFT routines are used for transformation from physical to spectral space and vice versa. Nonlinear terms are computed in a pseudo-spectral manner, i. e. only the derivatives of the primitive variables $q = [\rho, u, v, w, p, T]^T$ are computed in Fourier space and afterwards multiplied accordingly in physical space.

Inflow boundary conditions consist of characteristic boundary conditions for subsonic flow. Additionally, at the inflow input of periodic disturbances is possible providing means for turbulent inflow conditions and/or harmonic disturbance waves. At the wall boundary all velocities are set to 0 (no-slip) and the wall is chosen to be isothermal (cooled wall). Pressure on the wall is recovered by setting the wall-normal derivative equal to zero. Inhomogeneous boundary conditions on the wall are used to introduce perturbations through both periodic and steady suction and blowing. The nozzle flow of the jet actuators is modelled by a polynomial $\rho v(r) = R(1 - 6r^5 + 15r^4 - 10r^3)$ of $O5$ which guarantees smooth functions for the derivatives. Furthermore the jet exit flow can be skewed and pitched by arbitrary angles. This polynomial approximation of the jet flow has proven sufficiently accurate albeit small-scale interactions close to the nozzle edge as observed in experiments are not simulated. Figure 2(a) depicts the jet exit velocity profile approximation and the resulting azimuthal vorticity $\omega_\Theta = -\frac{\partial v(r)}{\partial r}$ in comparison to a circular pipe flow.

At the freestream boundary an exponential decay condition is used to eliminate perturbations and provide potential flow conditions.

Outflow boundary conditions are realized through a sponge zone containing a ramping function (relaminarization). Alternatively the grid can be stretched and a filter applied. In either case all deviations from initial conditions are fully damped before the domain exit is reached.

2.2 Problem-specific extensions

The regarded Jet-in-Crossflow computation constitutes a severe test to any numerical method as it exhibits multiple scale behaviour both in geometry and flow physics. Firstly, the jet orifices are usually comparatively small with respect to the domain dimensions influenced by the jet. Secondly, the jet-to-freestream velocity ratio is quite large depending on the objectives to be reached. For separation control, values between $R = 3 - 6$ are commonly used. Furthermore, flow control is used in low speed flight as encountered during take off and landing. Thus the freestream Mach numbers are in the range usually modelled by incompressible formulations of the Navier-Stokes equations whereas the high-speed jet flows exhibit compressibility

effects. The compressible equations show a decisively singular behaviour with decreasing Ma which can only be counteracted by deploying computationally expensive time-integration methods, i.e. implicit methods or small time-step size.

In order to overcome the aforementioned difficulties, grid transformation techniques have been incorporated allowing for grid compression and/or stretching in x and y direction. With respect to the present problem grid stretching in both x and y direction is employed. Step sizes and the rate of change of the step sizes are depicted in figure 2(b) for a typical mesh. This allows to resolve the jet exit with a sufficient number of grid points (6 per radius) in spite of its small extension $d \sim 1\delta^*$ where δ^* is the displacement thickness. Two methods to include artificial viscosity are imple-

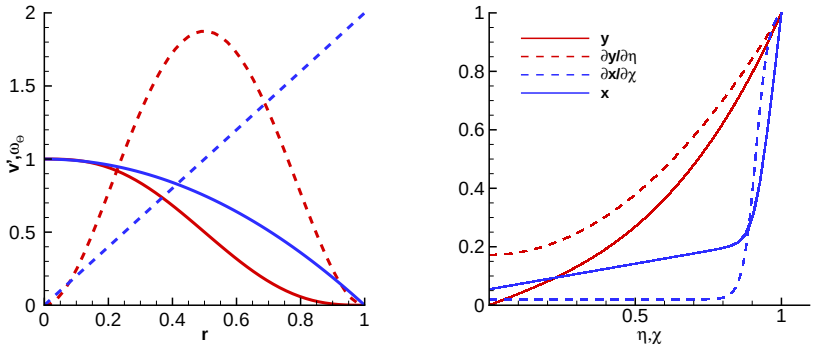

(a) (b)

Fig. 2. (a) Jet approximation: Solid lines are velocity profiles, dashed lines indicate vorticity. Red: Polynomial representation, blue: Hagen-Poiseuille profile. (b) Grid transformations

mented in the scheme. Either the spatial derivative stencil can be shifted alternately backwards and forwards in between time integration sub steps or a filter can be applied after each full Runge-Kutta step. Numerical tests have shown that large gradients at the jet-exit boundary lead to numerical instabilities which can not be suppressed by use of alternating stencils. Thus, it is necessary to add a filter scheme in x- and y-directions. As no subgrid scale model is used for unresolved scales of the flow, the filter has to be tailored suitably to allow all scales to pass which can be represented on the mesh otherwise the solution might be smoothed non-physically. Various compact filter schemes [9] have been examined and the respective transfer functions are compared in figure 3(a). It can be seen that the analytical transfer functions depend largely on the filter constant α rather than on the order of the filter. Nevertheless, higher-order schemes are by far superior in terms of keeping the order of the numerical approximation in space and time. After 10000 time steps both h^{10} order filters keep scales resolved on more than four mesh points almost unfiltered whereas the h^4 order filter exhibits a strong damping effect on the amplitudes of scales as large as eight mesh points. These wavenumbers are usually part of the

physical solution rather than being numerical artefacts and numerical damping is not desired. Therefore, a filter of order h^{10} finally has been implemented in combination with one-sided filters for near-wall points [5]. A test case scenario has been

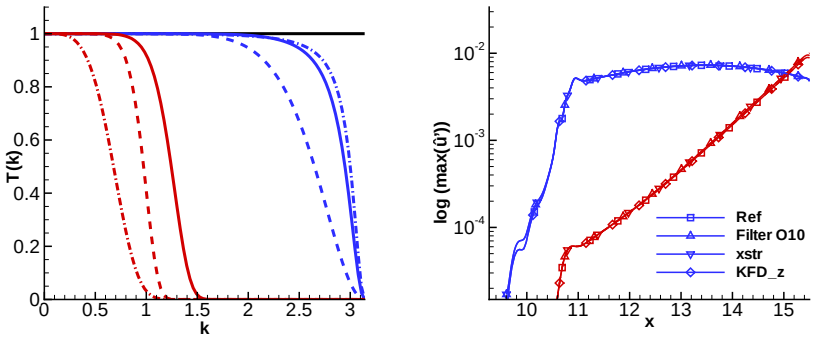

(a) (b)

Fig. 3. (a) Filter transfer function: Blue lines depict analytic transfer functions, red lines are exponential transfer functions. Solid: $h^{10}, \alpha = 0.49$, dashed: $h^{10}, \alpha = 0.4$, dash-dotted: $h^4, \alpha = 0.495$. (b) Test case for numerical scheme, blue lines represent 2D perturbations, red lines are 3D perturbations.

computed in order to test and verify the implemented extensions to the numerical scheme. Therefore, subharmonic laminar-turbulent transition on a flat plate with zero pressure gradient is simulated in accordance to Thumm [10]: one 2D and one 3D disturbance are introduced via a disturbance strip. The maximum amplitudes of the perturbed streamwise velocity is analysed in Fourier space in order to compare the outcome of the simulations for each wave. Results are shown in figure 3(b). The reference is taken from Thumm [10] and it can be seen that simulations with a stretched grid as well as simulations with a filter applied yield identical results to the reference. One more computation has been performed replacing the spectral discretization in spanwise direction by compact finite differences. Again agreement of the solution to the reference is excellent.

3 Results

Numerical simulations have been performed for two distinct Jet-in-Crossflow configurations which differ by the jet angles. The first configuration was chosen because it has been investigated both experimentally [8] and numerically [2]. The second setup was chosen with a configuration representative for separation control devices [3]. Freestream conditions are identical in both cases with inflow $Re = 165$ based on freestream velocity U_∞, kinematic viscosity ν and displacement thickness δ^*.

Freestream $Ma = 0.25$ which was chosen in order to avoid transonic effects. The mesh used in both cases consists of $800 \times 180 \times 128$ nodes in x, y and z direction, respectively. Grid stretching is applied in x and y direction and a filter is employed for the inclined jet. Initial step sizes are $\Delta x = 0.22$, $\Delta y = 0.1$ and $\Delta z = 0.2$ and the time step is $\Delta t = 0.0065$. Initial baseflow conditions represent a laminar boundary-layer flow on a flat plate with zero pressure gradient. The inhomogeneous boundary conditions mimic round hole jet nozzles with a diameter of $\delta^*/D = 1/3$. The freestream-to-jet-exit-velocity ratio is $R = 3$ in all cases.

3.1 Vertical jet

The vertical Jet-in-Crossflow simulation serves as test and reference case for succeeding simulations of skewed and inclined jet actuators. Computations have been carried out for 31 time units L_x/U_∞. Albeit this does not suffice to provide data for statistical analysis, it yields a good picture of the evolution of the perturbed flow field. The instantaneous flow is visualised in figure 4 by use of the λ_2 vortex detection method and streamwise velocity contour surfaces. Even if the jet itself is only modelled the typical structures of a jet in crossflow are simulated realistically. Such structures include the bending of the jet due to the oncoming freestream, formation of half-ring vortices in the strong shear layer on the top side of the jet as well as a horseshoe vortex which wraps around the nozzle and induces a near-wall high-speed streak in the wake behind the nozzle. Even though both the jet and the

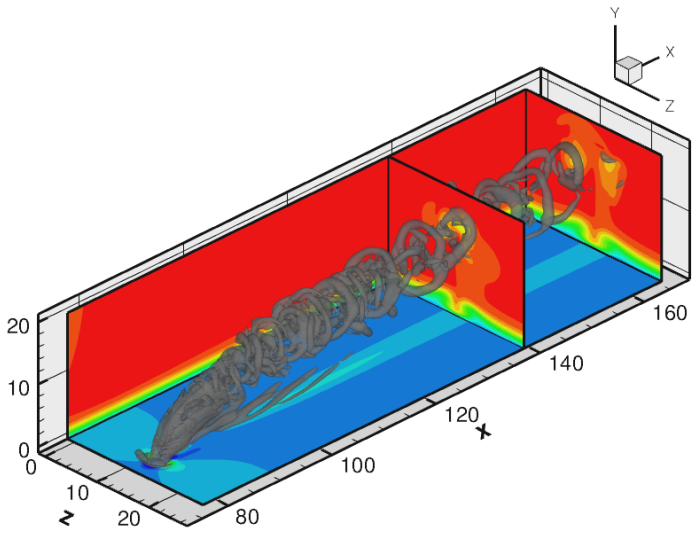

Fig. 4. Vertical Jet-in-Crossflow: Isosurfaces at $\lambda_2 = -0.01$, contours represent u

laminar boundary layer are initially steady the resulting flow regime becomes highly unsteady with the jet exhibiting unstable modes leading to the formation of periodic vortex rings on its top outside of the boundary layer. These rings merge and dissipate while convecting downstream. Close to the wall a different flow pattern can be observed. At the downstream side of the jet exit, fluid is drawn upstream and upwards rolling into two longitudinal vortices. As these vortices convect downstream they disperse and form a widening gap where high speed fluid is transported downwards. Again periodic instabilities are visible. Figure 5 shows downstream time averaged

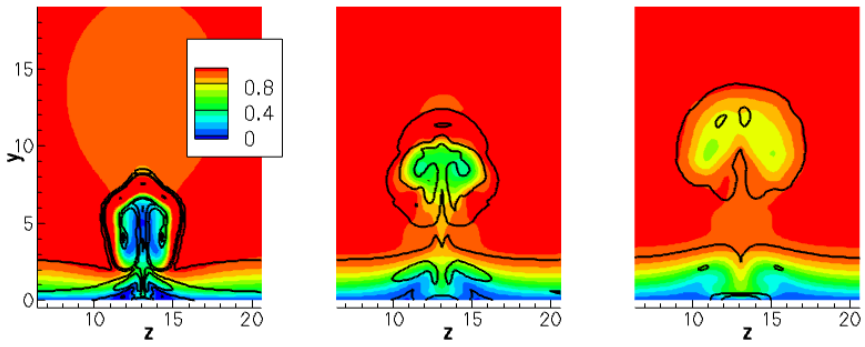

Fig. 5. Mean u contour levels and contour lines for mean ω at positions $\Delta x = 1.5D$, $\Delta x = 5D$ and $\Delta x = 9D$ (from left to right)

velocity and vorticity magnitude contours at stations $\Delta x = 1.5D$, $\Delta x = 5D$ and $\Delta x = 9D$ and demonstrates how the boundary layer low-speed layers roll up and a high-speed streak forms in the centreline behind the jet. Along the trajectory of the jet a vortex pair can be observed which merges into a half ring and is dissipated after a short distance downstream.

3.2 Inclined jet

Further simulations have been set up in accordance to an active flow-control-device configuration. For that the jet is inclined by $\alpha = 30^\circ$ and rotated against the freestream by $\beta = 30^\circ$. The peak jet-exit velocity magnitude is kept at $R = 3$. Simulations have been carried out on the same mesh for the same time period as the vertical jet simulations. An instantaneous snapshot of the vorticity system is shown in figure 6 by means of the λ_2 method and streamwise velocity contours. The very different flow pattern results from the skewing of the jet. Two longitudinal vortices establish in the flow and wrap around each other due to the induced velocities in the transversal plane. The development of a high-speed streak close to the wall takes place with an inclination to the centreline of the flow. The jet is bound closer to the wall because of the smaller vertical velocity component. The two longitudinal

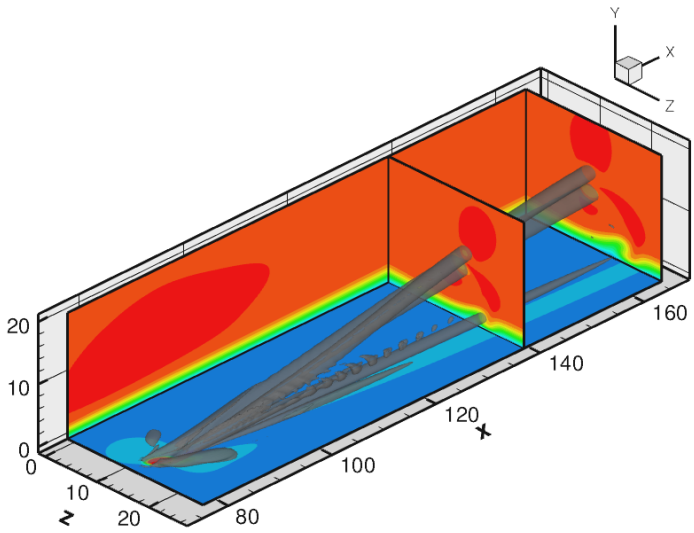

Fig. 6. Vertical Jet-in-Crossflow: Isosurfaces at $\lambda_2 = -0.001$, contours represent u

vortices seem not subject to instabilities at that point in time. They stretch rather well-defined downstream and upwards along the plate. By choice of a smaller λ_2 magnitude a third region of vorticity becomes visible which is bound to the wall. This wake region does exhibit instabilities as observed in the previous simulation. Figure 7 depicts the time averaged vorticity magnitude and streamwise velocity at downstream positions $\Delta x = 5D$, $\Delta x = 9D$ and $\Delta x = 23D$, respectively. The oncoming freestream deflects the jet in both spanwise and wall-normal direction. A strong shear layer develops on the top side of the jet. The sweep of the jet over the boundary layer results in the near-wall fluid layers being entrained upwards into the trajectory of the jet. The entrainment in combination with the deflection of the jet leads to the formation of a near-wall vortex-pair surrounded be the shear layer. This pair moves away from the wall while travelling downstream and it can be seen that the two vortices identified by the λ_2 method are the remaining cores of the vortex-pair after the rotational region has largely dissipated. The exchange of high- and low-speed layers inside the boundary layer is not as strong as in the case of the vertical jet.

3.3 Boundary layer control

As already mentioned in section 1, Jet-in-Crossflow configurations are investigated as a means to suppress boundary layer separation. This is to be achieved by increasing the wall friction through moving faster fluid layers closer to the wall. Figure 8 shows a comparison of the time-averaged wall-shear-stress distribution for the sim-

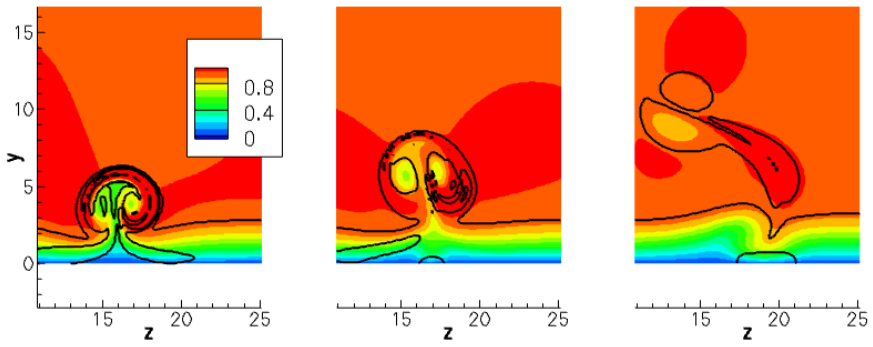

Fig. 7. Mean u contour levels and contour lines for mean ω at positions $\Delta x = 5D$, $\Delta x = 9D$ and $\Delta x = 23D$ (from left to right)

ulated cases. Both configurations lead to a net increase of wall shear stress in a confined stripe behind the jet. This region extends further in both downstream and spanwise direction when a vertical jet is used. Also the magnitudes of τ are larger for this case. Corresponding to the circles in figure 8, figures 9 and 10 depict the time-averaged u velocity profiles. These profiles are compared to the profiles of the unperturbed steady laminar flow. The velocity profiles show the mean-flow deformation in the wake. The wall gradients of the profiles along the wake centreline (numbers 1,3,5) are steeper and are similar to turbulent mean profiles. Outside the boundary layer a defect is visible which stems from the periodic sweeps of the vortex rings. Profiles measured on the edge or outside of the wake are not as strongly affected. The probe at position 2 can still see the sweep of the jet in the freestream whereas at station 5 no effects on the mean flow are recorded at all. Time-averaged streamwise velocity profiles for the inclined jet are illustrated in figure 10. The wall gradients do not increase as much as in the previous case at any measured station and the gain in momentum thus is not as large. At position 1 the profile exhibits layers of increased and decreased velocity corresponding to the deflection shear and the vortex-core position in wall-normal direction. At point 2 the momentum gain at the wall reaches a maximum and the streak just outside the boundary layer increases the streamwise speed. Further downstream the profile positioned along the wake centreline (number 3) still possesses a steeper gradient albeit already at a smaller inclination than point 2. Furthermore, the streak on top of the boundary layer widens and losses on its maximum speed are due to dissipation. The probe at position 4 on the other hand measures a profile containing an inflection point inside the boundary layer and a velocity-magnitude defect. The boundary layer is lifted upwards. Regarding the findings of the simulations some comments on the jet actuator's feasibility to suppress separation are to be made. Firstly, the simulations where done in a laminar boundary layer regime. Thus, the increase in momentum on the wall especially in case of a vertical jet stems mostly from introducing instabilities which the boundary layer is receptible to. These instabilities get amplified

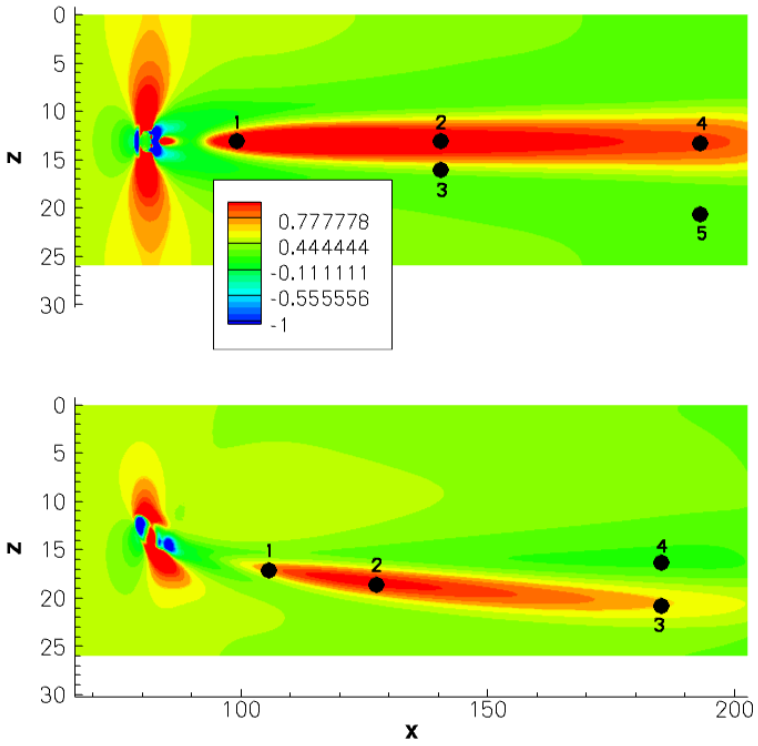

Fig. 8. Comparison of mean τ distribution. Top: vertical jet, bottom: inclined jet. Circles indicate probe position

and the boundary layer undergoes a transition from laminar to turbulent state. The jet mainly acts as obstacle and source for three-dimensional perturbations similar to a solid surface roughness element. The idea of the inclined jet is of a different nature. The jet not only serves as turbulator but is supposed to generate a very distinct longitudinal vortical motion in order to enhance the mixing of the fluid layers. Albeit the vortex is formed it does not lead to a larger increase of wall friction in the boundary layer than the vertical jet. The inclined jet might nontheless be the better option in case of a turbulent boundary layer regime where the blockage of a vertical jet does not deform the mean flow to the same amount as in the laminar case. Secondly, the parameters of the inclined jet may be altered to enhance the desired effect, either by increasing the velocity ratio and/or changing the pitch and skew angles.

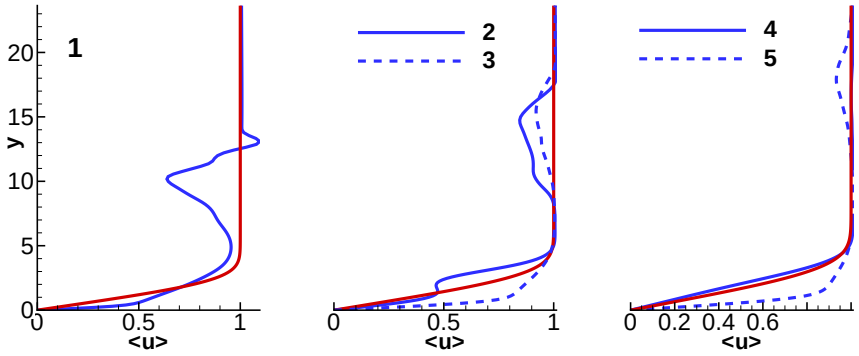

Fig. 9. Mean downstream velocity u profiles. Numbers correspond to the probe positions in fig. 8

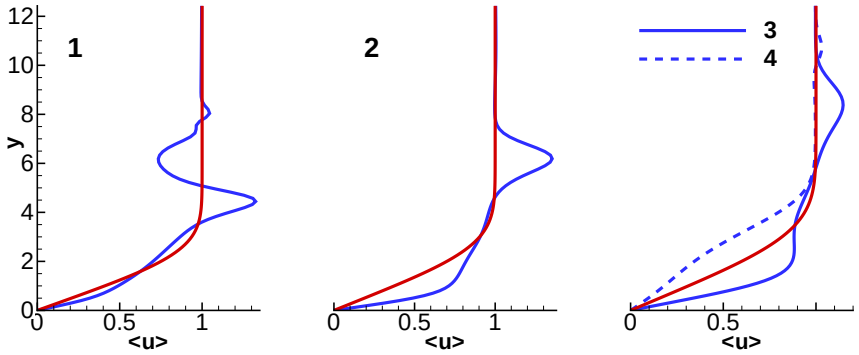

Fig. 10. Mean downstream velocity u profiles. Numbers correspond to the probe positions in fig. 8

3.4 Computational aspects

All simulations have been carried out on the NEC-SX9 supercomputer at HLRS Stuttgart. One node with 16 CPUs has been employed for all computations. Each computation consisted of one MPI process which was parallelized in z-direction employing NEC Microtasking shared-memory parallelization. Details of the algorithm can be found in [1]. All computations have employed a fully compact finite differencing scheme. Preliminary computations using a spectral ansatz in spanwise direction have shown to introduce unphysical wiggles due to the global representation of the jet. The fully compact discretization has additionally been found to benefit from an

increased time step limit. An overview of the main characteristics for the presented computations is shown in table 1. Memory usage accumulated to 24.576 GB for all

Case	Wall time [sec]	CPU time [sec]	time/TS/GP [μsec]	GFLOPS
VJ	33488	532228	0.60	230
INCJ	34294	545444	0.62	230
VJ – spec	33091	524314	0.59	231

Table 1. Computational resources for JIC simulations

cases and the vector operation ratio was at 99.67%. The slightly longer computational time in case of the inclined jet can be traced to the filter scheme. Due to the compact formulation one additional tridiagonal linear system of equations has to be solved for each spatial variable that is filtered. Filtering acquires about 1.5% of computational time for each variable. Thus an overall penalty of 3% has to be taken into account. The spanwise discretization does not show a siginificant difference between the spectral and compact schemes. The CPU time per time step and gridpoint averages to 0.60μsec which is about three times faster than computations on the NEC-SX8.

4 Conclusions

Simulations of two different Jet-in-Crossflow configurations have been carried out in order to investigate the effect on a laminar boundary layer at $Ma = 0.25$. The main characteristics, i.e. inflow Reynolds number Re and velocity ratio R have been kept constant. A reference case has been established by simulating a vertical jet geometry. In a subsequent simulation the jet has been skewed and inclined by values typically found in an active-flow-control device setup. The simulations gave insight into the generation of a jet-vortex system and wake perturbations. In case of a vertical jet a mean-flow deformation is achieved by instabilities in the wake leading to the onset of laminar-turbulent transition. An inclination and skew of the jet leads to the generation of a longitudinal vortex-pair which form the core of a region with increased vorticity. Instablities in the wake are not as dominant in this case. Thus, fluid layers in the boundary layer are mixed by an up- and downwash motion and only to a lesser extend by amplification of the unstable modes. The jets have been compared by means of measuring the mean wall-shear stress. A larger increase has been found for the vertical jet in the investigated scenario. Further simulations may include a variation of the pitch and skew angles of the jet as well as the velocity ratio. Of interest is also a variation of initial conditions towards a fully developed turbulent boundary layer. This can be achieved by exploiting the findings of the present work by using an array of vertical jets to perturb the flow sufficently and simulate the boundary layer laminar-turbulent transition process.

Acknowledgements

We thank the Höchstleistungsrechenzentrum Stuttgart (HLRS) for provision of supercomputing time and technical support within the project "LAMTUR".

References

1. A. Babucke. Direct numerical simulation of a serrated nozzle end for jet-noise reduction. In M. Resch, editor, *High Performance Computing in Science and Engineering 2007*. Springer.
2. S. Bagheri, P. Schlatter, P. J. Schmid, and D. Henningson. Global stability of a jet in crossflow. *J. Fluid Mech.*, 624:33–44, 2009.
3. M. Casper, C. J. Kähler, and R. Radespiel. Fundamentals of boundary layer control with vortex generator jet arrays. In *4th Flow Control Conference*, number AIAA 2008-3995.
4. D. A. Compton and J. P. Johnston. Streamwise vortex production by pitched and skewed jets in a turbulent boundary layer. *AIAA Journal*, 30(3):640–647, 1992.
5. D. V. Gaitonde and M. R. Visbal. Further Development of a Navier-Stokes Solution Procedure Based on Higher-Order Formulas. In *37th AIAA Aerospace Science Meeting & Exhibit*, number AIAA 99-0557.
6. G. Godard and M. Stanislas. Control of a decelerating boundary layer. Part 3: Optimization of round jets vortex generators. *Aerospace Science and Technology*, 10:455–464, 2006.
7. J. P. Johnston and M. Nishi. Vortex generator jets – a means for flow separation control. *AIAA Journal*, 28(6):989–994, 1990.
8. R. M. Kelso, T. T. Tim, and A. E. Perry. An experimental study of round jets in cross-flow. *J. Fluid Mech*, 306:111–144, 1996.
9. S. K. Lele. Compact finite difference schemes with spectral-like resolution. *Journal of Comp. Physics*, 103:16–42, 1992.
10. A. Thumm. *Numerische Untersuchung zum laminar-turbulenten Strömungsumschlag in transsonischen Grenzschichtströmungen*. PhD thesis, Universität Stuttgart, 1991.